

Dust outflows and inner gaps generated by massive planets in debris disks

Amaya Moro-Martín¹ and Renu Malhotra²

amaya@as.arizona.edu; renu@lpl.arizona.edu

ABSTRACT

Main sequence stars are commonly surrounded by debris disks, formed by cold far-IR-emitting dust that is thought to be continuously replenished by a reservoir of undetected dust-producing planetesimals. We have investigated the orbital evolution of dust particles in debris disks harboring massive planets. Small dust grains are blown out by radiation pressure, as is well known; in addition, gravitational scattering by the giant planets also creates an outflow of large grains. We describe the characteristics of this large-particle outflow in different planetary architectures and for different particle sizes. In addition, the ejection of particles is responsible for the clearing of dust inside the orbit of the planet. We study the efficiency of particle ejection and the resulting dust density contrast inside and outside the orbit of the planet, as a function of the planet’s mass and orbital elements and the particle size. We discuss its implications for exo-planetary debris disks and for the interpretation of in-situ dust detection experiments on space probes traveling in the outer solar system.

Subject headings: circumstellar matter — interplanetary medium — Kuiper Belt — methods: n-body simulations — planetary systems

1. Introduction

Debris disks are disks of dust that surround many main sequence stars. They were discovered by the IRAS satellite in the 1980’s (Aumann et al. 1984; Gillett 1986) and they are preferentially detectable at infrared wavelengths, where the dust re-radiates the light absorbed from the star. Stars harboring debris disks are too old to have remnants of the primordial disk from which the star itself once formed. This is because the dust grain removal processes, such as the Poynting-Robertson (P-R) effect and solar wind drag, act on timescales much shorter than the age of the star, indicating that such “infra-red excess stars” harbor a reservoir of undetected planetesimals producing dust by mutual collisions or by evaporation of comets scattered close to the star (Backman & Paresce 1993). The spectroscopy of systems like β -Pictoris supports this interpretation (e.g. Knacke et al. 1993;

¹Department of Astrophysical Sciences, Princeton University, Princeton, NJ 08544, USA

²Department of Planetary Sciences, University of Arizona, 1629 E. University Boulevard, Tucson, AZ 85721, USA

Pantin, Lagage & Artymowicz 1997). It seems clear, therefore, that planetesimals are present in these systems. But what about massive planets? High-resolution images of some of these debris disks have revealed the presence of density structure (see Koerner 2001 for a review) and dynamical models have shown that planets can sculpt the dust disks, creating gaps, arcs, rings, warps and clumps of dust (e.g. Roques et al. 1994; Liou & Zook 1999; Mouillet et al. 1997; Wyatt et al. 1999; Moro-Martín & Malhotra 2002; Kuchner & Holman 2003). The combination of both, the very high resolution imaging at long wavelengths and theoretical dynamical models can provide interpretation of the disks’ structure in terms of planetary architectures. This approach has been used in the interpretation of high resolution millimeter interferometry observations of the Vega system (Wilner et al. 2002) and of the submillimeter images of the ϵ Eridani system (Ozernoy et al. 2000; Quillen & Thorndike 2002). Recent observations with the *Spitzer* MIPS instrument have confirmed that out of 26 FGK field stars known to have planets by radial velocity studies, 6 show $70\mu\text{m}$ excess at $3\text{-}\sigma$ confidence level, implying the presence of cool material (<100 K) located beyond 10 AU (Beichman et al. 2005). These stars, with a median age of 4 Gyr, are the first to be identified as having both well-confirmed planetary systems and well-confirmed IR excesses (Beichman et al. 2005). In addition, the first results from the *Spitzer* FEPS Legacy project indicate that inner gaps¹ appear to be common in cold Kuiper Belt-like disks (Kim et al. 2005). These disks show excesses at $70\mu\text{m}$ but not at $24\mu\text{m}$, indicating again the presence of cool dust (<100 K) located beyond 10 AU. The lack of $24\mu\text{m}$ emission yields an upper limit to the amount of warm dust inside 10 AU; this upper limit is 10^{-3} to 10^{-2} times the lower limit for the mass in the corresponding cold disk. Because the lifetime of the dust particles due to P-R drag is of the order of 1 Myr, it is expected that the density contrast would be erased on this timescale. Kim et al. (2005) suggest that a possible explanation for these inner gaps is that one or more massive planets are dynamically depleting, via gravitational scattering, dust particles generated by an outer belt of planetesimals. All these observations are providing increasing evidence that debris disks and massive planets co-exist around many sun-like stars.

In this paper we report some new results based on numerical modeling regarding the depletion of large dust particles in debris disks by the gravitational perturbations of massive planets. The numerical models used to carry out this study are briefly described in §2. The ejected particles form an “outflow” whose properties (angular confinement, velocity and efficiency of ejection) are characterized in §3.1 as a function of the planet’s mass and orbital elements, and the particle size. The high efficiency of ejection, together with the possible high frequency of debris disks harboring massive planets, suggest that these outflows may be a common phenomenon, whose implications are described in §3.2. The ejection of particles is also responsible for the depletion of dust interior to the orbit of the planet, creating a density contrast that can be measured directly in spatially resolved images or indirectly through the modeling of the spectral energy distribution (SED) of the debris disk. To aid in the interpretation of such observations, in §4 we study the density contrast inside and outside the orbit of the planet, as a function of the planet’s mass and orbital elements and the particle size. Finally, §5

¹In this paper a “gap” is an inner depletion zone in the dust disk interior to the planet’s orbit, not an annular depletion zone around the planet’s orbit.

summarizes our results.

2. The numerical models

We numerically solve the equations of motion of dust particles generated in a debris disk, analogous to the solar system’s Kuiper Belt. We use a modified version called SKEEL of the multiple time step symplectic method SyMBA (Duncan, Levison & Lee 1998; Moro-Martín & Malhotra 2002). Our models include the combined effects of solar gravity, solar radiation pressure, the P-R effect and solar wind drag, and the gravitational forces of planets. We model the solar system with 7 planets (excluding Mercury and Pluto, and including the mutual perturbations of the planets), and we model hypothetical extra-solar planetary systems with single planets of different masses, semimajor axes and eccentricities (see Tables 1, 2 and 3 for a complete list of models). For some of these systems, the parent bodies of the dust particles are assumed to be distributed in orbits with semimajor axis between 35 and 50 AU, eccentricities such that the perihelion distances are between 35 and 50 AU, and inclinations between 0 and 17° , in approximate accord with current estimates of the orbital distribution of the classical Kuiper Belt (Malhotra et al. 2000; Brown 2001). For other systems, the dust-producing planetesimals are randomly distributed in a thinner disk with $a=35\text{--}50$ AU, $e=0\text{--}0.05$ and $i=0\text{--}0.05$ radians. In all our models, the initial values of mean anomaly (M), longitude of ascending node (Ω) and argument of perihelion (ω) were randomly distributed between 0 and 2π . We run models for different particle sizes, referred to in terms of their β value, which is the dimensionless ratio of the radiation pressure force and the gravitational force. For spherical grains,

$$\beta = (3L_*/16\pi GM_*c)(Q_{pr}/\rho s), \quad (1)$$

where L_* and M_* are the stellar luminosity and mass; for a solar-type star, $\beta=5.7 \times 10^{-5} Q_{pr}/\rho s$, where ρ and s are the density and radius of the grain in cgs units (Burns, Lamy & Soter 1979). Q_{pr} is the radiation pressure coefficient, a function of the physical properties of the grain and the wavelength of the incoming radiation; the value we use is an average, integrated over the solar spectrum. [For the correspondence between β and the particle size see Fig. 5 in Moro-Martín, Wolf & Malhotra (2005).] The sinks of dust included in our numerical simulations are (1) ejection into unbound orbits, (2) accretion into the planets, and (3) orbital decay to less than 0.5 AU heliocentric distance (0.1 AU for the models with a single planet located at 1 AU). A detailed description of the numerical algorithm used to integrate the equations of motion is given in Moro-Martín & Malhotra (2002).

3. Dust outflows from debris disks

Radiation pressure arises from the interception by the dust particles of the momentum carried by the incident stellar photons; it makes the orbits of the dust particles change immediately upon release from their parent bodies (i.e., the meter-to-kilometer size dust-producing planetesimals). For parent bodies in circular orbits, small grains with $\beta > 0.5$ are forced into hyperbolic orbits as soon

as they are released. If the parent bodies’ orbits are eccentric, ejection occurs for $\beta > 0.5(1 \mp e)$ for a particle released at perihelion or aphelion, respectively. In the solar system these particles are known as β -meteoroids (Zook & Berg 1975). These small dust particles leave the system in a “disk wind”, whose angular extent is determined by the inclinations of the parent bodies; this is because radiation pressure is a radial force which does not change the inclinations of the dust particles after their release.

Grains larger than the “blow-out” size, on the other hand, remain on bound orbits upon release, and their orbital evolution is the subject of our study. Their dynamical evolution is affected by the P-R effect, which tends to circularize and shrink their orbits, forcing these particles to slowly drift in toward the central star (Burns, Lamy & Soter 1979). If no planets were present, the final fate of these dust particles would be to drift all the way into the star until they sublimate. Other removal processes may include mutual grain collisions and collisions with interstellar grains, which may comminute the grains to sizes small enough to be blown away by radiation pressure. [The studies reported here do not include collisional effects; for an estimate of the limitations of our models we refer to Moro-Martín & Malhotra (2002 and 2003).] When planets are present the story changes: (a) the trapping of particles in mean motion resonances (MMRs) with the planets causes an accumulation of particles at resonant semimajor axes; and (b) sufficiently massive planets can scatter and eject dust particles out of the planetary system. In the case of dust produced in the Kuiper Belt in our solar system, about 80–90% of the dust grains are ejected by close encounters with the giant planets (mainly Jupiter and Saturn), a few percent accrete onto the planets, and the remaining 10–20% drift all the way into the Sun (Liou, Zook & Dermott 1996; Moro-Martín & Malhotra 2003; see also Table 1). Thus, in addition to the afore-mentioned β -meteoroids, an outflow of larger particles produced by gravitational scattering from planets also exists.

3.1. Dependence on planetary architecture and particle size

We have explored the characteristics of the large particle outflow and its dependence on planetary architecture and particle size. For the solar system architecture, it is known that the majority of KB dust particles are ejected by Jupiter and Saturn (Liou, Zook & Dermott 1996; Moro-Martín & Malhotra 2003). Motivated by this, we have modeled hypothetical planetary systems consisting of a single planet and a KB-like dust source. These models explore a range of planetary masses ($M_p/M_{Jup}=0.03, 0.1, 0.3, 1, 3, \text{ and } 10$), orbital semimajor axis ($a=1, 5.2, 10, 20 \text{ and } 30 \text{ AU}$), and eccentricities ($e=0, 0.1, 0.2, 0.3, 0.4, 0.5$) (see Tables 1, 2 and 3).

Fig. 1 shows examples of the escaping² particle trajectories for the solar system case, projected

²Our definition of “escaping” is that the particles reach a distance 1000 AU from the star (see Fig. 3 to 6); at that point, we stop integrating their orbits. This is not quite equivalent to the precise criterion for ejection, which would be that a particle velocity exceed the escape velocity. However, our numerical studies find that the particles that reach 1000 AU, 30-60% (depending on their β) are in hyperbolic orbits, and more than 90% have orbital eccentricity $e > 0.98$. This means that even though some of the particles are still bound by the time they reach 1000 AU, it is very likely that they

in the ecliptic plane (XY; left panel), and in the RZ plane (right panel; where R is the in-plane heliocentric distance and Z is the off-plane out-of-ecliptic distance). These examples are of particles that reach at least 1000 AU and had their last encounter with Jupiter. We see that Jupiter creates a fan-like outflow, mainly confined to the ecliptic, where the trajectories are in the counterclockwise (prograde) direction. The distributions of eccentricity, inclination and perihelion of these Jupiter-ejected particles are presented in Fig. 2. The histograms show that all the particles are either in or very close to hyperbolic orbits; that the scattering rarely changes the inclination of the particles by more than 15 degrees (see also column 9 in Table 1); and that few of the ejected particles leave on orbits of perihelion interior to Jupiter’s orbit.

For the single planet models, Fig. 3–6 show the velocities of the escaping particles at 1000 AU projected in the XY (ecliptic) plane (left) and in the XZ plane (right). At large heliocentric distances the outflow is radial and symmetric, except when the planet is in an eccentric orbit (Fig. 6); the projection in the XZ plane shows that it is largely confined to the ecliptic for Jupiter-mass planets (or smaller), and becomes less confined as the planet mass increases. The angular confinement to the disk can also be seen in Fig. 7 and 8, in the distribution of orbital inclination for the ejected particles, and in column 9 of Tables 1, 2 and 3. This angular confinement is not obvious a priori because the ejection of the particles is due to gravitational scattering, a process that does not necessarily preserve the inclination of the orbits.

In Tables 1–3, we give a list of the single-planet and multiple-planet models that we have simulated (a total of 126 models). Also included in these tables are the statistical results for the fates of the dust particles in each model. We have performed simulations for several solar system models with the same or similar initial conditions of the dust parent bodies and the results indicate that a conservative estimate of the uncertainty in n_{1000} , owing to the chaotic dynamics of dust orbital evolution, is $\sim 10\%$ of the initial number of particles.

Fig. 9 and 10 show the percentage of particles that are gravitationally scattered out from the system, and the velocity at infinity of the ejected particles, as a function of the planet’s mass, semimajor axis and eccentricity, and the particle size. We find the following dependencies (the parentheses show the values explored by our models).

- *Particle sizes* ($\beta=0.00156, 0.00312, 0.00625, 0.0125, 0.025, 0.044, 0.1, 0.2$ and 0.4): It is expected that gravitational scattering is dependent to some extent on the particle size as smaller particles (larger β) migrate past the planet faster, therefore decreasing their probability of ejection. The top panel of Fig. 9 shows that: (1) For a $1M_{Jup}$ planet, the efficiency of ejection decreases as β increases, reaching a minimum at $\beta\sim 0.1-0.2$ and increasing thereafter. As mentioned above, the decrease in efficiency is expected because the particle P-R drift velocity is larger for larger β . The increase in efficiency for even larger β is probably due to the fact that radiation pressure

will also be set on hyperbolic orbits within a few orbits, either by subsequent scattering from the planets or due to small additional perturbations not included in our models.

is starting to contribute to the ejection of the particles. (2) The effect described above is more significant for close-in planets (1 AU), i.e. when the particle is deeper in the potential well of the star. (3) Planets $>3M_{Jup}$ in circular orbits between 1 AU and 30 AU eject $>80\%$ of the particles that go past, independently of the particle size. In addition, from the top panel of Fig. 10, we see that there is an increase in \bar{v}_∞ as the particle size decreases (β increases), which is more pronounced when the perturbing planet is closer to the star. The distributions of particle inclinations in Fig. 2 and 7 show that the angular confinement of the ejected particles is similar for all particle sizes. This is not surprising because the inclination perturbation in gravitational scattering is independent of particle size, as particle masses are more than 30 orders of magnitude smaller than the masses of the planets.

- *Planet semimajor axis* (1, 5.2, 10, 20 and 30 AU): We find that the average dust outflow velocity is larger in the presence of close-in planets than more distant planets of the same mass (see top panels of Fig. 10). This trend is clearly seen in the left panel of Fig. 11; the slope of the line corresponds to approximately $\bar{v}_\infty \propto a_{pl}^{-0.5}$, and is consistent with an analytical calculation by Murray, Weingartner & Capobianco (2003).
- *Planet mass* (0.03, 0.1, 0.3, 1, 3, and $10M_{Jup}$): The right panel of Fig. 11 shows only a weak dependence on the mass of the planet of the average particle ejection velocity; this is somewhat in contrast with the theoretical prediction, $v_\infty \propto M_{pl}^{1/4}$ (Murray, Weingartner & Capobianco 2003). The magnitude of the ejection velocity, $\sim 3 \text{ km s}^{-1}$, in the Jupiter-mass single-planet models (blue line in the top left panel of Fig. 10) is higher than the numerical result in Murray, Weingartner & Capobianco (2003), but agrees better with their analytical estimate. Their analysis, however, assumes that the particle ejection takes place after only a single planetary encounter, whereas our simulations show that typically ejections occur after many planetary encounters. (In our simulations, we track the planetary encounters of dust particles within 3.5 Hill-radius distance from each planet. The number of such encounters that ejected particles suffer is on the order of $10\text{--}10^4$, with the lower range being more typical in models with more massive planets, $3\text{--}10 M_{Jup}$). In addition to this complexity, it is important to remember that the effect of the planet's orbital elements and mass on the outflow parameters (velocity and confinement to the plane) is not only direct, via the close encounters, but also indirect, as the particles encounter the planet with a history of evolution in the MMRs that can change the initial orbital elements of the particles and therefore affect their subsequent dynamical evolution. As an example, the eccentricity distributions of the soon-to-be-ejected particles near the planet show that for the 1 and $3 M_{Jup}$ models, $e \sim 0.4\text{--}0.5$, but for $10 M_{Jup}$, $e < 0.2$.

The distribution of inclinations in Fig. 7 shows that for a planet at 1 and 5.2 AU, the angular confinement of the outflow to the disk is affected by the planet's mass; the more massive the planet the less confinement the outflow has. However, the parameter that is most strongly dependent on the planet's mass is the number of ejected particles. The bottom left panel of Fig. 9 shows that there is a sharp increase in ejection efficiency when the planet mass increases from $0.3 M_{Jup}$ to $1 M_{Jup}$: planets $\lesssim 0.1 M_{Jup}$ do not eject a significant number of particles, whereas planets $>3 M_{Jup}$ eject $>90\%$ if located between 1–30 AU. A $1 M_{Jup}$ planet at 5–30 AU ejects

about 80% of the particles, and about 60% if located at 1 AU.

- *Planet eccentricity* (0, 0.1, 0.2, 0.3, 0.4 and 0.5): Large planet eccentricities create an asymmetric outflow oriented along the major axis of the planet’s orbit. The number of particles ejected in the apoastron direction exceeds that in the periastron direction by a factor of ~ 5 for $e=0.5$ (see Fig. 6). The asymmetry is due to the fact that the planet spends more time near apoastron and therefore the probability of encounter with a dust particle is higher near apoastron. Fig. 8 and 10 show that the inclinations and the average velocity of the ejected particles at infinity are not affected by the planet’s eccentricity. The efficiency of ejection, however, decreases significantly as the planet’s eccentricity increases: for a $1 M_{Jup}$ planet at 5 AU it decreases from $\sim 80\%$ to $\sim 30\%$ when the planet eccentricity is increased from 0 to 0.5 (see bottom right panel in Fig. 9). It is of interest to note that many of the known exo-planets to date have large orbital eccentricities (Marcy et al. 2003); our models predict that the large particle outflow will be asymmetric in these cases.
- *Comparison with Solar System*: The single-planet analog of the solar system (i.e. only Jupiter in a circular orbit at 5.2 AU) produces a somewhat higher velocity outflow compared with the actual multi-planet solar system. This is mainly due to the effect of Saturn in our solar system: having a larger semimajor axis, Saturn intercepts a fraction of the KB dust grains as they evolve inward due to the P-R drag and ejects them at a somewhat lower velocity, thus depressing the mean velocity of the outflow.

3.2. Implications of dust particle outflows

There are several significant implications of this large-particle outflow.

3.2.1. Exo-planetary debris disks and planet formation environment

Stellar surveys show that at least 15% of A-K main sequence stars are surrounded by debris disks, and that the far-infrared excess decreases with stellar age, dropping from about 50% to about 15% after approximately 500 Myr. But these samples are sensitivity-limited, and therefore the occurrence of debris disks could be higher (Lagrange, Backman & Artymowicz 2000 and references therein). Stellar radial velocity surveys indicate that about 7% of the FGK main sequence stars have a Saturn or Jupiter-mass planet within 3 AU (Marcy 2003). Even though the correlation between the presence of planets and debris disks is not known yet, our studies suggest these large-particle dust outflows may be a common phenomena in planetary systems that harbor debris disks. This is of interest because: (a) These large-particle dust outflows *may contribute significantly or even dominate the clearing of circumstellar debris in planetary systems*. Hitherto, the main processes that have been considered for such clearing are stellar winds, radiation pressure, sublimation, and collisions. The latter reduce the size of the dust particles until they are small enough to be blown away by radiation pressure. However,

as our models indicate, gravitational scattering by giant planets following orbital decay by P-R drag is also significant, and in some cases may be a dominant process, ejecting 50–90% of the dust grain population.

(b) These outflows should be added to the list of processes that *link the interplanetary environment to the galactic environment of a star*. Planetary systems are prime sites for large particle formation. As such, they can contaminate the immediate vicinity of star-forming regions through this large particle outflow, and thus affect the particle size distribution of their local ISM. It is likely, therefore, that large particle outflows from extra-solar planetary systems may be a source of the large interstellar particles that have been detected in the interplanetary medium.

The presence of an outflow in an exo-planetary system and its detectability will strongly depend on the orbital characteristics of the planet and the orientation of the system. For face-on systems, the expected surface brightness of the dust outflow will be very low, making it very hard to detect astronomically as a radial extension of the debris disk. Additionally, the lack of velocity information from usual infrared measurements will not allow to distinguish between an outflow and a bound disk.

The face-on optical depth of a disk composed of grains of radius a and observed at frequency ν is given by (Backman & Paresce 1993): $\tau_{\perp}(r,\nu) = \sigma(r)(\xi a\nu/c)^q$; where $\sigma(r)$ cm^2/cm^2 is the face-on fractional geometric surface density; it is equal to the surface density $n(r)$, multiplied by the geometric cross section of the grain, $\sigma(r) = n(r)\pi a^2$. ξ is the ratio between the critical wavelength λ_0 up to which the grain absorbs and emits radiation efficiently) and the grain radius a , and depends on the grain properties (e.g. $\xi \equiv \lambda_0/a \sim 2\pi$, $1/2\pi$ and 1 , for strongly, weakly and moderately absorbing materials; we will use $\xi \sim 1$). q is the power law index of the emissive efficiency ϵ , such that for $\lambda < \lambda_0$, $\epsilon \sim 1$, but for longer wavelengths the emissive efficiency decreases as $\epsilon = \epsilon_0(\lambda_0/\lambda)^q$; for the intermediate size regime, where a is larger than λ_{peak} of the incoming radiation (absorbs efficiently) but smaller than λ_{peak} of the grain thermal emission (emits inefficiently), $q=1$. And c is the velocity of light.

We can estimate the surface density $n(r)$ (cm^{-2}) at a distance r from the central star from mass conservation by equating the mass that is produced in time dt , $dN = dprf_{ej}dt$, with the mass that crosses the annulus of radius r in time dt , $dN = n(r)2\pi r v dt$. dpr is the dust production rate in particles per second; f_{ej} is the fraction of particles that are ejected (our numerical studies find $f_{ej} \sim 50\text{--}90\%$); and v is the velocity of the particles at distance r , for large distances we will take $v \approx v_{esc} = (2GM_{\odot}/r)^{1/2}$. Solving for $n(r)$ and substituting into $\sigma(r)$,

$$\tau_{\perp}^{outflow}(r,\nu) = \sigma(r)\left(\frac{\xi a\nu}{c}\right)^q = \frac{dprf_{ej}}{2\pi r(2GM_{\odot}/r)^{1/2}}\pi a^2\left(\frac{\xi a\nu}{c}\right)^q. \quad (2)$$

We can estimate the optical depth of the solar system's outflow using the KB dust production rates derived by Landgraf et al. (2002), which are based on *Pioneer 10* and *11* measurements and for the Kuiper Belt gives $dpr \sim 2 \times 10^{14}$ particles/s (for particles between 0.01 and 6 mm). Because the size distribution is very steep, one can assume that most of the detections are caused by particles just above the detection threshold, i.e. particles with $a \approx 5 \mu\text{m}$. For this particle size, $\beta \approx 0.05$ and $f_{ej} \approx 0.8$, and the optical depth at $60 \mu\text{m}$ ($\nu = 5 \times 10^{12} \text{Hz}$) will then be $\tau_{\perp}^{outflow}(r,\nu) = 2.6 \times 10^{-14}/r^{1/2}$ (where r is in AU). We can compare this to the optical depth of the Kuiper Belt (bound) disk. From Fig.

11 in Moro-Martín & Malhotra (2002) we can get the surface density that corresponds to a fictitious dust production rate of 100 particles per 1000 years, $n \approx 300$ particles/AU². Scaling up this density to account for the dust production rate found by Landgraf et al. (2002), we find that $n \approx 8.4 \times 10^{-2}$ particles/cm², $\sigma \approx 6.6 \times 10^{-8}$, so that $\tau_{\perp}^{disk} \approx 5.5 \times 10^{-9}$. For the solar system, the ratio of the two optical depths is then $\sim 10^{-6}$. Other models for the Kuiper Belt dust disk give $\sigma \approx 10^{-6}$ (15 times larger than our value; Backman, Dasgupta & Stencel 1995). It is estimated that for a system at 30 pc, the 70 μm *MIPS* array in *Spitzer* will be able to detect a disk with $\sigma \approx 3 \times 10^{-6}$ (D. Backman, private communication). This means that in order to see the Kuiper Belt dust disk the dust production rate will need to be increased by a factor of ~ 3 in Backman’s models, or a factor of ~ 45 in our models (using Landgraf’s *dpr*). But in order to see the outflow it will need to be increased by a factor of $\sim 6 \times 10^6$ (Backman’s) or 9×10^7 (ours). In any case, this increase will make the bound disk be optically thick. In other words, for an optically thin debris disk (where our dynamical models are valid), this outflow is very unlikely to be detected. For younger and more massive edge-on systems, after the giant planets have already formed, it may be possible to detect the outflow out of the plane. In this geometry, the signature of the off-plane outflow will be clearer against the fainter background. However, our dynamical models are not valid in this high-density regime where collisional effects dominate over P-R drag. It is possible that such an outflow may have already been detected with the Advanced Meteor Orbit Radar, which senses plasma signatures produced by extra-terrestrial dust particles ablating in the Earth’s atmosphere: Taylor, Baggaley & Steel (1996) and Baggaley (2000) claim that the main discrete source seems to coincide in direction with β Pictoris.

3.2.2. Interpretation of in-situ dust detections made by space probes

Recent Ulysses and Galileo dust experiments have led to the surprising discovery of interstellar grains sweeping through the solar system deep within the heliosphere (Grun, Zook & Baguhl 1993). Previously, interstellar grains could only be studied by extinction and polarization measurements of optical starlight, not sensitive to grains larger than 0.3 microns because of their small contribution to the optical cross section, and by infrared emission. These in-situ detections allowed us for the first time to study the mass distribution of interstellar grains within the heliosphere, leading to the surprising discovery of a population of large particles ($> 10^{-16}$ kg, Grun et al. 1994) that are 30 times more massive than the interstellar grains that cause stellar extinction. This finding implies that more mass is locked up in large grains locally than has been estimated from the astronomical measurements. The gas-to-dust ratio derived from astronomical measurements (400–600) is found to be much larger than the value of ~ 100 derived from the in-situ detections, implying that the local interstellar cloud exceeds cosmic abundances (Frisch et al. 1999). These very important results rely critically on the correct identification of the origin of the dust grains. This identification is based on a geometrical argument: the direction the grains are coming from, with interstellar grains coinciding with the flow of neutral helium through the solar system; and a dynamical argument: the impact velocity and the expectation that only interstellar grains are on unbound hyperbolic orbits (Grun, Zook & Baguhl 1993). Under the current understanding, the sources of meteoroids in interplanetary space and their orbital properties

are assumed as follows: Asteroids: low eccentricity and inclination; Comets: high eccentricity and inclination; Kuiper Belt: low eccentricity and inclination; and Interstellar: hyperbolic, and aligned with the direction of flow of the interstellar gas. However, we have shown in this paper that $\sim 80\text{--}90\%$ of large Kuiper Belt grains ($\beta < 0.5$) are gravitationally scattered outward by Jupiter and Saturn into hyperbolic orbits; therefore there is the potential of misinterpreting these escaping interplanetary particles as interstellar. In addition, other sources exist such as comets, Asteroid Belt and Trojan asteroids. Due to radiation pressure, some of the dust particles released at those locations will be set on Jupiter crossing orbits, so in principle close encounters with Jupiter could take place resulting on hyperbolic orbits. In the future, we plan to study whether or not these particles may have been detected by Ulysses and Galileo. For the analysis of future in-situ dust detections in the outer solar system, such as with the *Cassini* Cosmic Dust Analyzer and the *Interstellar Probe*, it will be important to keep in mind the existence of the large-particle outflow of solar system dust to correctly identify the origin of the massive fast moving particles, whether interplanetary or interstellar. It has been recently announced that the analysis of the ion charge signals in the *Cassini* dust detector, together with geometric and kinematic considerations, have led to the identification of an interstellar flux at 0.8 AU that is in agreement with the flux measured by Ulysses at 3 AU at the same time (Altobelli et al 2003). But any dust detections by Cassini outside Jupiter’s orbit have not yet been reported.

4. On how debris disks with inner gaps signal the presence of massive planets

Recent GTO and *FEPS* observations with the *Spitzer* MIPS instrument suggest that debris disks and giant planets co-exist and that inner gaps appear to be common in cold Kuiper Belt-like disks (Beichman et al. 2005 and Kim et al. 2005). In view of these observations, it is interesting to study the efficiency of particle ejection (§3.1) and the resulting dust density contrast inside and outside the orbit of the planet, as a function of the planet’s mass and orbital elements and the particle size. It is important to keep in mind, however, that the modeling presented here does not consider the effect of particle collisions, which together with P-R drag could also be responsible for the opening of an inner gap in the dust disk (Wyatt 2005).

If the particles were drifting inward at a constant rate, as set by P-R drag, the ratio n_{in}/n_{1000} (from Tables 1, 2 and 3) would directly give us an estimate of the density contrast inside and outside the inner boundary of the disk. However, the trapping of particles in MMRs with the planet halts the P-R drift, increasing the number density of particles in that region. The density contrast, therefore, can only be estimated using the radial density profiles that result from the numerical simulations. Fig. 12 shows some of these profiles for a representative set of models. These results, keeping in mind the uncertainties due to the fact that we are modeling the dynamical evolution of a small number of test particles ($N \sim 100$), can help us estimate what planet masses and semimajor axes may be responsible for the inner gaps that are inferred indirectly from the disks’ SEDs, or in few cases, that are seen directly in spatially resolved images. For planets located at 1–30 AU with masses of $1\text{--}10M_{Jup}$, the ratio between the density outside and inside the orbit of the planet is $\gtrsim 40$, whereas for planet masses

of $0.03\text{--}0.3M_{Jup}$, this ratio is in the range 3–10. The models show that the radius of the inner depleted region, r_{gap} , depends on the mass and the eccentricity of the planet. In Table 4 we show that for the models with planets in circular orbits, $r_{gap}\sim 0.8\times a_{pl}$ for $1\text{--}3M_{Jup}$ and $\sim 1.2\times a_{pl}$ for $10M_{Jup}$. The three bottom panels of Fig. 12 show that for planets with eccentricities in the range 0.3–0.5, the surface density decreases more smoothly and consequently the dust disk would not present a sharp inner edge.

5. Conclusions

When a massive planet is located interior to a belt of dust-producing planetesimals, dynamical models have shown that as the dust particles drift inward due to P-R drag, they get trapped in MMRs with the planet, and this well-known effect can sculpt the dust disk creating rings, warps and azimuthal asymmetries. In addition to the trapping in MMRs, gravitational scattering with the planet is responsible for the depletion of dust inside the orbit of the planet. Although this is also a well known effect, to our knowledge it has not been studied in detail in the past. In this paper we have shown that the ejected dust particles form an “outflow”, whose angular confinement, velocity and symmetry depend on the planet’s mass and orbital elements, as well as the particle size. The high efficiency of ejection (for planet masses $\gtrsim 1M_{Jup}$), together with the possible high frequency of debris disks harboring massive planets, suggest that these outflows may be a common phenomenon. If this is the case, they may contribute significantly or even dominate the clearing of circumstellar debris in planetary systems, enriching the immediate vicinity of star-forming regions with large dust particles and affecting therefore the particle size distribution of their local ISM. In addition, we have seen how the ejection of particles is responsible for the clearing of dust inside the orbit of the planet, creating a density contrast that can be measured directly in spatially resolved images or indirectly through the modeling of the SED of the debris disk. Indeed, recent *Spitzer* observations suggest that debris disks and giant planets co-exist and that inner gaps appear to be common in cold Kuiper Belt-like disks (Beichman et al. 2005, Kim et al. 2005). To aid in the interpretation of these observations, we have studied the efficiency of particle ejection and the resulting dust density contrast inside and outside the orbit of the planet, as a function of the planet’s mass and orbital elements and the particle size.

Acknowledgments

We thank Hal Levison for providing the SKEEL computer code, Alberto Noriega-Crespo, Dana Backman, George Rieke, Re’em Sari and Mark Sykes for useful discussion, and the anonymous referee for very helpful comments on how to improve the manuscript. This work is part of the *Spitzer* FEPS Legacy project (<http://feps.as.arizona.edu>). We acknowledge NASA for research support (contract 1224768 administered by JPL and grants NAG5-10343 and NAG5-11661), and IPAC, the *Spitzer* Science Center and the Max-Planck-Institute in Heidelberg for providing access to their facilities. AMM is also supported by the Lyman Spitzer Fellowship at Princeton University.

REFERENCES

- Altobelli, N., Kempf, S., Srama, R. et al. 2003, in *Astrophysics of Dust, Estes Park, Colorado* (eds A.N. Witt).
- Aumann, H.H., Beichman, C.A., Gillett, F.C. et al. 1984, *ApJ*, 278, L23.
- Backman, D.E. & Paresce, F. 1993, in *Protostars and Planets III* (eds E.H. Levy & J.I. Lunine) 1253 (Univ. Arizona Press, Tucson).
- Backman, D. E., Dasgupta, A., & Stencel, R. E. 1995, *ApJ*, 450, L35.
- Backman, D. E. 2004, *ASPC*, 324, 9.
- Baggaley, W.J. 2000, *J.Geophys.Res.*, 105, 10353.
- Beichman C.A., Bryden, G., Rieke, G.H. et al. 2005, 622, 1120.
- Brown, M.E. 2001, *AJ*, 121, 2804.
- Burns, J.A., Lamy, P.L. & Soter, S. 1979, *Icarus*, 40, 1.
- Duncan, M.J., Levison, H.F. & Lee, M.H. 1998, *AJ*, 116, 2067.
- Frisch, P.C., Dorschner, J.M., Geiss, J. et al. 1999, *ApJ*, 525, 492.
- Gillett, F.C. 1986, in *Light on Dark Matter* (ed. F.P. Israel) 61 (Dordrecht:Ridel).
- Grun, E., Zook, H.A., Baguhl, M. et al. 1993, *Nature*, 362, 428.
- Grun, E., Gustafson, B., Mann, I. et al. 1994, *Astron. Astrophys.*, 286, 915.
- Kim, J.S., Hines, D.C., Backman, D.E et al. 2005, submitted to *ApJ*.
- Knacke, R.F., Fajardo-Acosta, S.B., Telesco, C.M. et al. 1993, *ApJ*, 418, 440.
- Koerner, D.W. 2001, in *ASP Conf. Ser. 231, Tetons 4: Galactic Structure, Stars, and the Interstellar Medium* (eds C.E. Woodward, M.D. Bica & J.M Shull) 563 (San Francisco:ASP).
- Kuchner, M.J. & Holman, M.J. 2003, *ApJ*, 588, 1110.
- Lagrange A.-M, Backman, D.E & Artymowicz, P. 2000, in *Protostars and Planets IV* (eds V. Mannings, A.P. Boss & S.S. Russell) 639 (Univ. Arizona Press, Tucson).
- Landgraf, M., Liou, J.-C., Zook, H.A, & Grün, E. 2002, *AJ*, 123, 2857.
- Liou, J.C., Zook, H.A. & Dermott, S.F. 1996, *Icarus*, 124, 429.
- Liou, J.C. & Zook, H.A. 1999, *AJ*, 118, 580.

- Malhotra, R., Duncan, M. J., & Levison, H. F. 2000, in *Protostars and Planets IV* (eds V. Mannings, A.P. Boss & S.S. Russell) 1231 (Univ. Arizona Press, Tucson).
- Marcy, G.W., Butler R.P., Fischer D.A. & Vogt S.S. 2003, in *Scientific Frontiers in Research on Extrasolar Planets* (eds Deming & Seager) ASP Conference Series vol. 294.
- Moro-Martín, A. & Malhotra, R. 2002, *AJ*, 124, 2305.
- Moro-Martín, A. & Malhotra, R. 2003, *AJ*, 125, 2255.
- Moro-Martín, A., Wolf, S. & Malhotra, R. 2005, *ApJ*, 621, 1079.
- Murray, N., Weingartner, J.C. & Capobianco, P., 2003, astro-ph/0309805.
- Mouillet, D., Larwood, J.D., Papaloizou, J.C.B. & Lagrange, A.M. 1997, *MNRAS*, 292, 896.
- Ozernoy, L.M., Gorkavyi, N.N., Mather, J.C. & Taidakova, T.A. 2000, *ApJ*, 537, 147.
- Pantin E., Lagage, P.O. & Artymowicz, P. 1997, *Astron. Astrophys.*, 327, 1123.
- Quillen, A.C. & Thorndike S. 2002, *ApJ*, 578, L149.
- Roques, F., Scholl, H., Sicardy, B. & Smith, B.A. 1994, *Icarus*, 108, 37.
- Taylor, A.D., Baggaley, W.J. & Steel, D.I. 1996, *Nature*, 380, 323.
- Wilner, D.J., Holman, M.J., Kuchner, M.J. & Ho, P.T.P. 2002, *ApJ*, 569, L115.
- Wyatt, M.C., Dermott, S.F., Telesco, C.M. et al. 1999, *ApJ*, 527, 918.
- Wyatt, M.C. 2005, *A&A*, 433, 1007.
- Zook, H.A. & Berg, O.E. 1975, *Space Sci.*, 23, 183.

Table 1.

M_{pl} (M_{Jup})	a	e	β	n_{in} (km/s)	n_{col}	$n_{1000}(n_{ejec})$	$\bar{v}_\infty(\sigma_{\bar{v}_\infty})$	$(\langle v_z^2 \rangle / \langle v_{xy}^2 \rangle)^{1/2}$
Solar	System		0.00156	1	4	95(29)	2.3(1.8)	0.10
1	1	0		6	5	89(72)	4.8(4.5)	0.20
3	1	0		19	1	80(62)	3.4(3.5)	0.002
10	1	0		5	0	95(80)	4.3(5.0)	0.33
1	5	0		15	0	85(33)	2.9(1.9)	0.15
3	5	0		10	0	90(44)	3.3(2.7)	0.35
10	5	0		4	0	96(50)	1.5(0.8)	0.36
1	30	0		1	0	69
3	30	0		0	1	69
10	30	0		0	2	69
Solar	System		0.00312	4	2	94(26)	1.7(1.0)	0.13
1	1	0		10	5	85(80)	5.5(3.9)	0.10
3	1	0		8	1	91(60)	4.3(3.7)	0.40
10	1	0		1	1	98(83)	4.2(4.7)	0.37
1	5	0		12	0	88(49)	3.2(2.7)	0.24
3	5	0		17	1	82(40)	3.5(2.8)	0.31
10	5	0		2	0	98(46)	1.7(1.8)	0.44
1	30	0		2	0	68
3	30	0		2	0	68
10	30	0		0	2	68
Solar	System		0.00625	5	6	89(33)	2.2(1.8)	0.21
1	1	0		9	8	83(74)	5.8(4.1)	0.10
3	1	0		14	6	80(68)	5.6(4.3)	0.21
10	1	0		7	0	93(83)	4.1(3.9)	0.43
1	5	0		19	1	80(42)	3.0(2.4)	0.26
3	5	0		12	0	88(43)	3.3(3.4)	0.32
10	5	0		7	0	93(35)	2.3(2.7)	0.34
1	30	0		8	0	62
3	30	0		0	1	69
10	30	0		0	3	67
Solar	System		0.0125	8	3	89(32)	2.2(1.9)	0.08
1	1	0		17	2	81(74)	5.0(3.7)	0.08
3	1	0		5	8	87(82)	5.9(3.1)	0.15

Table 1—Continued

M_{pl} (M_{Jup})	a	e	β	n_{in} (km/s)	n_{col}	$n_{1000}(n_{eject})$	$\bar{v}_{\infty}(\sigma_{\bar{v}_{\infty}})$	$(\langle v_z^2 \rangle / \langle v_{xy}^2 \rangle)^{1/2}$
10	1	0		5	0	95(81)	3.8(3.7)	0.38
1	5	0		14	0	86(63)	2.5(1.5)	0.10
3	5	0		8	0	92(39)	2.7(2.0)	0.36
10	5	0		3	0	97(48)	2.0(2.1)	0.43
1	30	0		4	0	66
3	30	0		5	0	65
10	30	0		1	2	67
Solar	System		0.025	15	1	84(31)	2.0(1.7)	0.09
1	1	0		23	1	76(65)	5.9(4.2)	0.08
3	1	0		7	10	83(79)	7.0(3.2)	0.13
10	1	0		7	0	93(81)	3.7(3.4)	0.39
1	5	0		17	0	83(56)	2.5(1.9)	0.14
3	5	0		14	3	83(42)	2.7(2.0)	0.35
10	5	0		9	0	91(55)	2.4(2.4)	0.45
1	30	0		11	0	59
3	30	0		2	1	67
10	30	0		1	4	65
Solar	System		0.044	19	3	78(28)	2.1(1.6)	0.08
1	1	0		39	3	58(53)	5.8(4.7)	0.10
3	1	0		7	2	91(89)	6.5(3.8)	0.06
10	1	0		11	0	89(78)	4.6(5.6)	0.31
1	5	0		25	0	75(53)	2.6(1.6)	0.09
3	5	0		12	0	88(52)	3.7(3.0)	0.27
10	5	0		5	0	95(48)	2.0(2.2)	0.41
1	30	0		11	1	58
3	30	0		0	3	67
10	30	0		2	1	67
Solar	System		0.1	21	3	76(48)	2.0(1.5)	0.05
1	1	0		43	2	55(53)	7.0(4.8)	0.10
3	1	0		18	5	77(75)	7.9(4.1)	0.06
10	1	0		5	1	94(90)	5.7(4.1)	0.14
1	5	0		38	1	61(37)	3.0(2.0)	0.11
3	5	0		14	2	84(68)	2.9(1.7)	0.16

Table 1—Continued

M_{pl} (M_{Jup})	a	e	β	n_{in} (km/s)	n_{col}	$n_{1000}(n_{ejec})$	$\bar{v}_{\infty}(\sigma_{\bar{v}_{\infty}})$	$(\langle v_z^2 \rangle / \langle v_{xy}^2 \rangle)^{1/2}$
10	5	0		10	0	90(55)	2.2(1.6)	0.35
1	30	0		11	2	57
3	30	0		3	0	67
10	30	0		2	2	66
Solar	System		0.2	15	0	85(42)	2.4(1.7)	0.1
1	1	0		47	3	50(48)	6.8(4.1)	0.07
3	1	0		17	3	80(79)	9.8(4.7)	0.06
10	1	0		0	9	91(89)	9.1(4.0)	0.02
1	5	0		32	1	67(52)	3.1(2.0)	0.11
3	5	0		8	1	91(79)	3.5(1.8)	0.07
10	5	0		0	5	95(81)	4.1(2.1)	0.04
1	30	0		3	1	66
3	30	0		2	0	68
10	30	0		0	0	70
Solar	System		0.4	11	0	89(58)	3.3(2.1)	0.10
1	1	0		39	5	56(53)	11.5(6.8)	0.13
3	1	0		7	5	88(86)	11.0(6.9)	0.10
10	1	0		0	7	93(92)	12.2(6.5)	0.03
1	5	0		24	1	75(67)	4.0(2.6)	0.13
3	5	0		5	0	95(90)	4.6(2.5)	0.07
10	5	0		0	5	95(90)	5.6(2.9)	0.05
1	30	0		0	0	70
3	30	0		0	0	70
10	30	0		0	0	70

The first planet in J labeled "S system (fr Almanac : column lis the dust p

inner cut-off distance (0.1 AU from the central star for the models with the planet at 1 AU, and 0.5 AU for the rest); n_{col} is number of particles that collide with the planet(s); n_{1000} is number of particles that reach 1000 AU; n_{ejec} is number of particles on hyperbolic orbits ($E > 0$); \bar{v}_∞ is the mean value of the velocity at infinity, $(2E)^{1/2}$, of the particles on hyperbolic orbits, and $\sigma_{\bar{v}_\infty}$ is its standard deviation. In the Solar system models, initial conditions of the dust particles are derived from assumed parent bodies having a distribution similar to the Solar system's KBOs, with a in the range 35–50 AU, e such that perihelion distance is in the range 35–50 AU and i in the range 0–17°. For all single-planet models, the parent bodies were assumed distributed with a in the range 35–50 AU, e in the range 0–0.05 and i in the range 0–0.05 radians. In each model we simulated 100 dust particles, with the exception of the single-planet models with the planet at 30 AU; in the latter models, we simulated 70 particles from parent bodies assumed to have a in the range 40–50 AU, since closer objects would be destabilized by the planet's perturbations.

Table 2.

M_{pl} (M_{Jup})	a	e	β	n_{in} (km/s)	n_{col}	$n_{1000}(n_{ejec})$	$\bar{v}_{\infty}(\sigma_{\bar{v}_{\infty}})$	$(\langle v_z^2 \rangle / \langle v_{xy}^2 \rangle)^{1/2}$
0.03	1	0	0.044	100	0	0(0)
0.1				98	2	0(0)
0.3				89	4	7(4)	5.2(3.7)	0.11
1				39	3	58(53)	5.8(4.7)	0.10
3				7	2	91(89)	6.4(3.8)	0.06
10				11	0	89(78)	4.6(5.6)	0.31
0.03	5.2	0	0.044	100	0	0(0)
0.1				100	0	0(0)
0.3				78	0	22(11)	2.9(2.0)	0.05
1				25	0	75(53)	2.6(1.6)	0.09
3				12	0	88(52)	3.7(3.0)	0.27
10				5	0	95(48)	2.0(2.2)	0.41
0.03	10	0	0.044	100	0	0(0)
0.1				95	1	4(1)	1.1	1.36
0.3				71	0	29(11)	2.0(1.3)	0.10
1				18	1	81(40)	1.8(1.1)	0.08
3				12	0	88(56)	2.0(1.1)	0.14
10				1	0	99(44)	1.5(0.9)	0.16
0.03	20	0	0.044	99	1	0(0)
0.1				98	0	2(1)	3.4	0.00
0.3				56	2	42(11)	1.7(1.1)	0.06
1				20	0	80(28)	1.2(0.7)	0.13
3				6	1	93(40)	1.3(0.8)	0.10
10				0	0	100(35)	1.1(0.6)	0.12
0.03	30	0	0.044	70	0	0
0.1				68	0	2
0.3				41	0	29
1				11	1	58
3				0	3	67
10				2	1	67

The column headings are the same as Table 1, but in these models the parent bodies of the dust particles are assumed to have an orbital distribution similar to the solar system’s KBOs, with a in the range 35–50 AU, e such that periastron distance is in the range 35–50 AU, and i in the range 0–17°.

Table 3.

M_{pl} (M_{Jup})	a	e	β	n_{in} (km/s)	n_{col}	$n_{1000}(n_{ejec})$	$\bar{v}_{\infty}(\sigma_{\bar{v}_{\infty}})$	$(\langle v_z^2 \rangle / \langle v_{xy}^2 \rangle)^{1/2}$
1	5	0	0.044	25	0	75(53)	2.6(1.6)	0.09
		0.1		22	1	77(50)	2.4(1.7)	0.11
		0.2		36	1	63(42)	2.6(1.6)	0.15
		0.3		32	1	67(30)	2.7(1.7)	0.10
		0.4		55	1	44(27)	2.8(1.9)	0.11
		0.5		65	0	35(20)	3.1(1.9)	0.10
1	10	0	0.044	18	1	81(40)	1.8(1.1)	0.08
		0.1		24	2	74(33)	1.6(1.1)	0.09
		0.2		19	1	80(37)	1.7(1.2)	0.09
		0.3		31	0	69(23)	1.7(1.3)	0.12
		0.4		45	2	53(19)	2.2(1.2)	0.10
		0.5		56	1	43(16)	1.8(0.9)	0.15
1	20	0	0.044	20	0	80(28)	1.2(0.8)	0.13
		0.1		18	0	82(19)	1.7(1.7)	0.16
		0.2		27	1	72(13)	1.5(0.9)	0.16
		0.3		27	0	73(18)	1.6(1.3)	0.16
		0.4		38	0	62(22)	2.2(2.2)	0.16
		0.5		47	1	52(14)	1.8(1.3)	0.22

The ir

Table 4.

$M_{pl}(M_{Jup})$	a	e	β	r_{gap} (AU)	r_{gap}/a
1	1	0	0.00156	0.8	0.8
3	1	0		0.8	0.8
10	1	0		1.2	1.2
1	5	0		4.2	0.8
3	5	0		4.8	0.9
10	5	0		6.4	1.2
1	30	0		25.2	0.8
3	30	0		25.2	0.8
10	30	0		32.2	1.1
1	1	0	0.00312	0.8	0.8
3	1	0		0.8	0.8
10	1	0		1.2	1.2
1	5	0		4.4	0.8
3	5	0		4.6	0.9
10	5	0		6.4	1.2
1	30	0		25.2	0.8
3	30	0		25.2	0.8
10	30	0		35.5	1.2
1	1	0	0.00625	0.8	0.8
3	1	0		0.8	0.8
10	1	0		1.2	1.2
1	5	0		4.4	0.8
3	5	0		4.6	0.9
10	5	0		6.1	1.2
1	30	0		25.2	0.8
3	30	0		25.2	0.8
10	30	0		37.2	1.2
1	1	0	0.0125	0.8	0.8
3	1	0		0.8	0.8
10	1	0		1.1	1.1
1	5	0		4.4	0.8
3	5	0		4.1	0.8
10	5	0		6.1	1.2
1	30	0		25.2	0.8

Table 4—Continued

$M_{pl}(M_{Jup})$	a	e	β	r_{gap} (AU)	r_{gap}/a
3	30	0		25.2	0.8
10	30	0		37.2	1.2
1	1	0	0.025	0.8	0.8
3	1	0		0.8	0.8
10	1	0		1.2	1.2
1	5	0		4.4	0.8
3	5	0		4.4	0.8
10	5	0		6.4	1.2
1	30	0		24.0	0.8
3	30	0		25.2	0.8
10	30	0		37.2	1.2
1	1	0	0.044	0.8	0.8
3	1	0		0.8	0.8
10	1	0		1.4	1.4
1	5	0		4.2	0.8
3	5	0		4.2	0.8
10	5	0		5.8	1.1
1	30	0		24.0	0.8
3	30	0		25.2	0.8
10	30	0		39.1	1.3
1	1	0	0.1	0.8	0.8
3	1	0		0.8	0.8
10	1	0		1.2	1.2
1	5	0		4.1	0.8
3	5	0		4.1	0.8
10	5	0		6.1	1.2
1	30	0		24.0	0.8
3	30	0		25.2	0.8
10	30	0		35.5	1.2
1	1	0	0.2	0.8	0.8
3	1	0		0.8	0.8
10	1	0		1.2	1.2
1	5	0		4.0	0.8
3	5	0		4.0	0.8

Table 4—Continued

$M_{pl}(M_{Jup})$	a	e	β	r_{gap} (AU)	r_{gap}/a
10	5	0		6.8	1.3
1	30	0		22.9	0.8
3	30	0		24.0	0.8
10	30	0		37.2	1.2
1	1	0	0.4	0.7	0.7
3	1	0		0.7	0.7
10	1	0		2.1	2.1
1	5	0		3.8	0.7
3	5	0		3.6	0.7
10	5	0		6.4	1.2
1	30	0		24.0	0.8
3	30	0		39.1	1.3
10	30	0		37.2	1.2

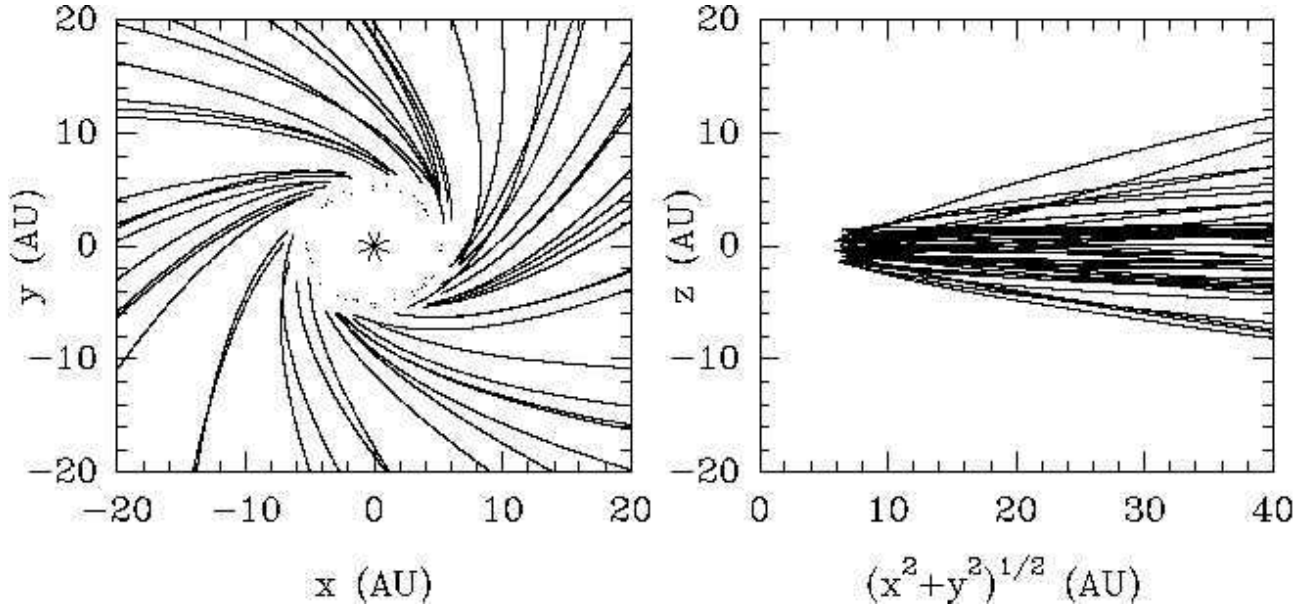


Fig. 1.— Trajectories of the particles that reach 1000 AU after scattering by Jupiter. These particles have $\beta=0.2$ and their paths are shown just after the last encounter with the planet. (left) in the XY plane; the dots represent the position of Jupiter at the time of last encounter; (right) in the RZ plane, where $R=(x^2+y^2)^{1/2}$ is the in-plane heliocentric distance and Z is the off-plane out-of-ecliptic distance.

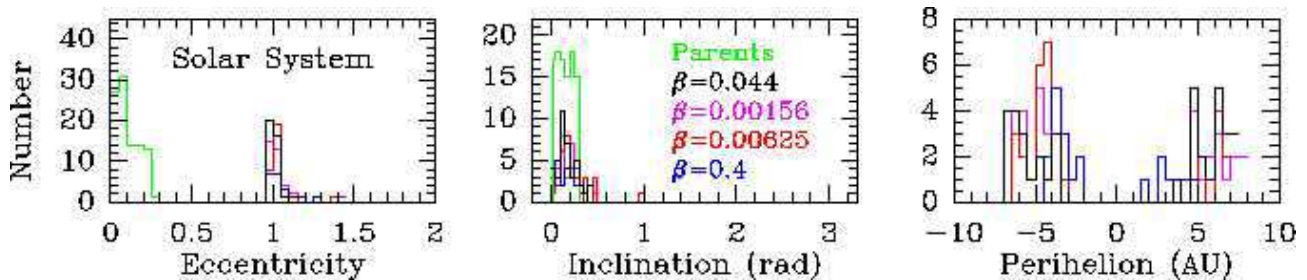


Fig. 2.— Distribution of eccentricity (left), inclination (center) and perihelion (right) of the particles ejected by Jupiter in the solar system models. Three different particles sizes are shown, corresponding to β -values of 0.044 (black), 0.00156 (magenta), 0.00625 (red) and 0.4 (blue). The green lines show the distributions for the parent bodies with $a=35-50$ AU, e such that perihelion $=35-50$ AU and $i=0-17^\circ$.

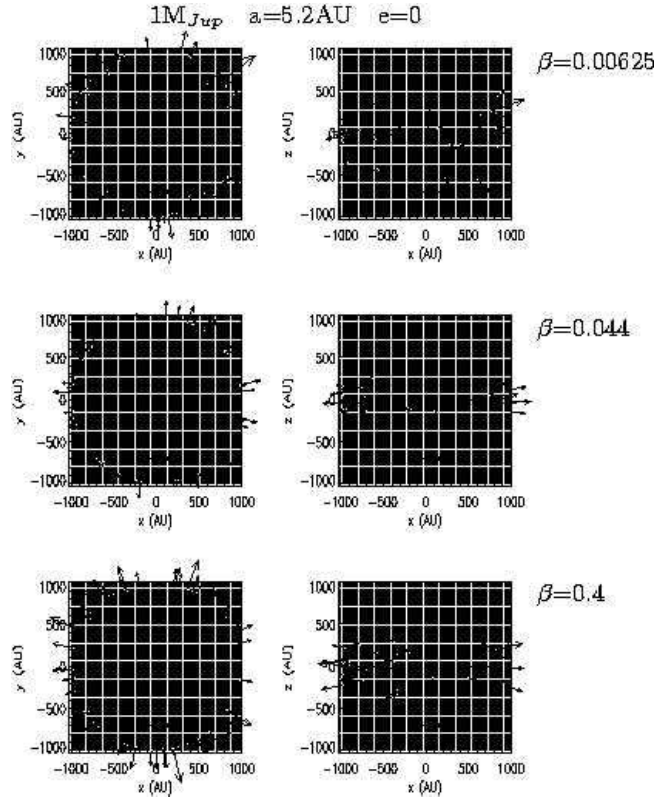


Fig. 3.— Escaping dust particles of three different sizes (i.e. three different β -values), shown in the XY plane (left) and XZ plane (right). These are models with a $1M_{Jup}$ planet with $a=5.2$ AU and $e=0$. The magnitude of the particle velocity at infinity is indicated by the length of the arrows; the velocity scale of 10 km/s is indicated by the size of the large arrow at the bottom-center in each panel. In all cases, the dust-producing planetesimals are randomly distributed with $a=35\text{--}50$ AU, $e=0\text{--}0.05$ and $i=0\text{--}0.05$ radians.

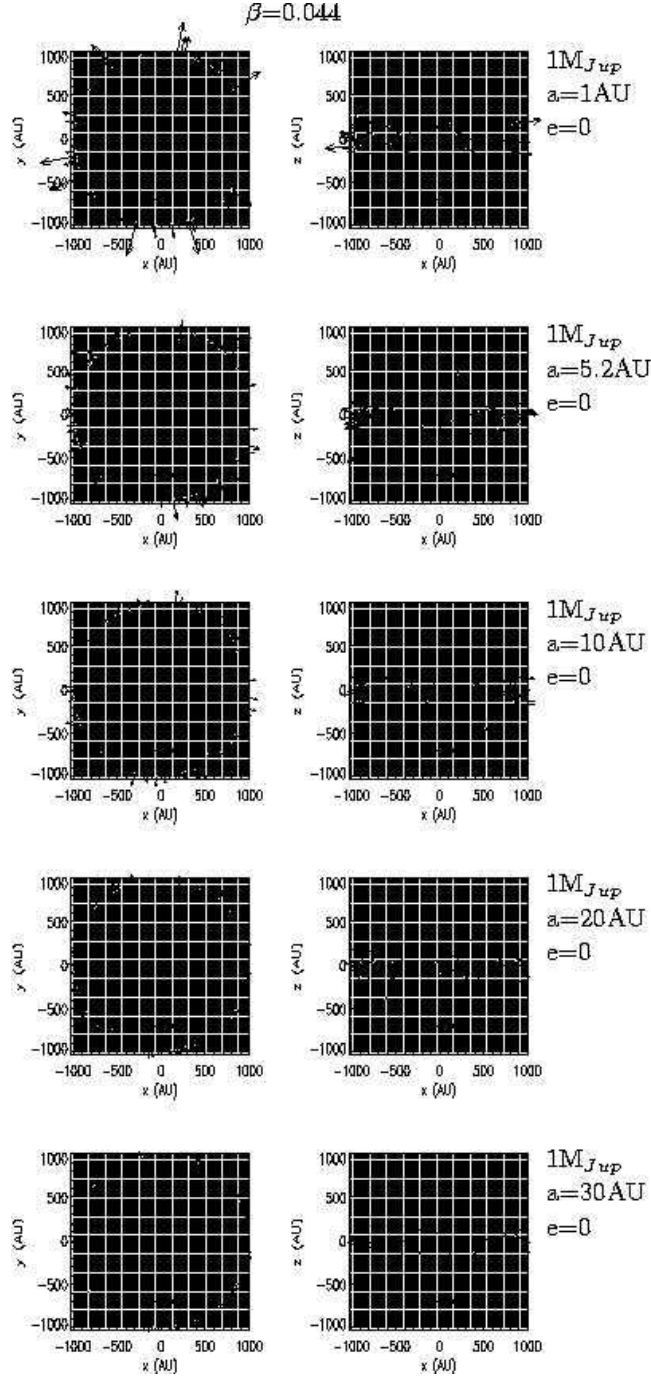


Fig. 4.— Escaping dust particles (with $\beta=0.044$) in five different planetary systems, shown in the XY plane (left) and XZ plane (right). From top to bottom, the panels correspond to models with a $1M_{Jup}$ planet in a circular orbit and with semimajor axis of 1 AU, 5.2 AU, 10 AU, 20 AU and 30 AU, respectively. The magnitude of the particle velocity at infinity is indicated by the length of the arrows; the velocity scale of 10 km/s is indicated by the size of the large arrow at the bottom-center in each panel. In all cases, the dust-producing planetesimals are randomly distributed with $a=35\text{--}50\text{AU}$, $q=35\text{--}50\text{AU}$ and $i=0\text{--}17^\circ$, similarly to the KBOs.

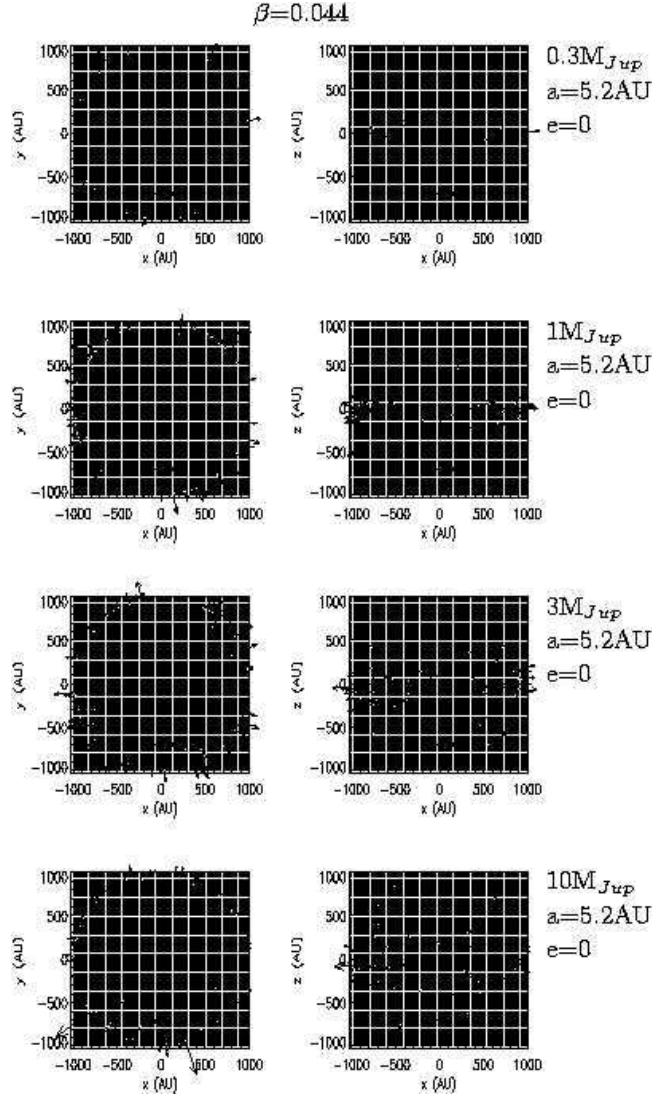


Fig. 5.— Escaping dust particles (with $\beta=0.044$) in four different planetary systems, shown in the XY plane (left) and XZ plane (right). From top to bottom, the panels correspond to models with a single planet with $a=5.2$ AU and $e=0$ and a mass of $0.3M_{Jup}$, $1M_{Jup}$, $3M_{Jup}$ and $10M_{Jup}$, respectively. The magnitude of the particle velocity at infinity is indicated by the length of the arrows; the velocity scale of 10 km/s is indicated by the size of the large arrow at the bottom-center in each panel. In all cases, the dust-producing planetesimals are randomly distributed with $a=35\text{--}50$ AU, $q=35\text{--}50$ AU and $i=0\text{--}17^\circ$, similarly to the KBOs.

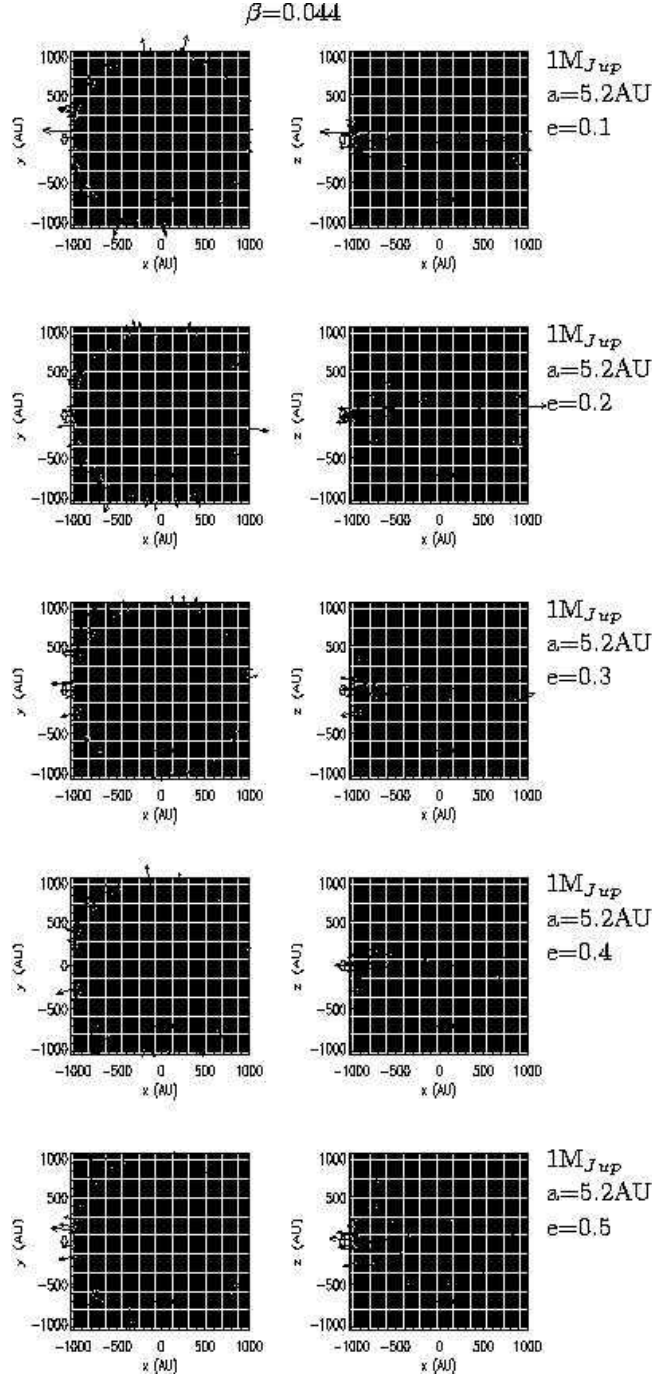


Fig. 6.— Escaping dust particles (with $\beta=0.044$) in five different planetary systems, shown in the XY plane (left) and XZ plane (right). From top to bottom, the panels correspond to models with a single $1M_{Jup}$ planet with $a=5.2$ AU and eccentricity of 0.1, 0.2, 0.3, 0.4 and 0.5, respectively. The magnitude of the particle velocity at infinity is indicated by the length of the arrows; the velocity scale of 10 km/s is indicated by the size of the large arrow at the bottom-center in each panel. In all cases, the dust-producing planetesimals are randomly distributed with $a=35\text{--}50$ AU, $q=35\text{--}50$ AU and $i=0\text{--}17^\circ$, similarly to the KBOs.

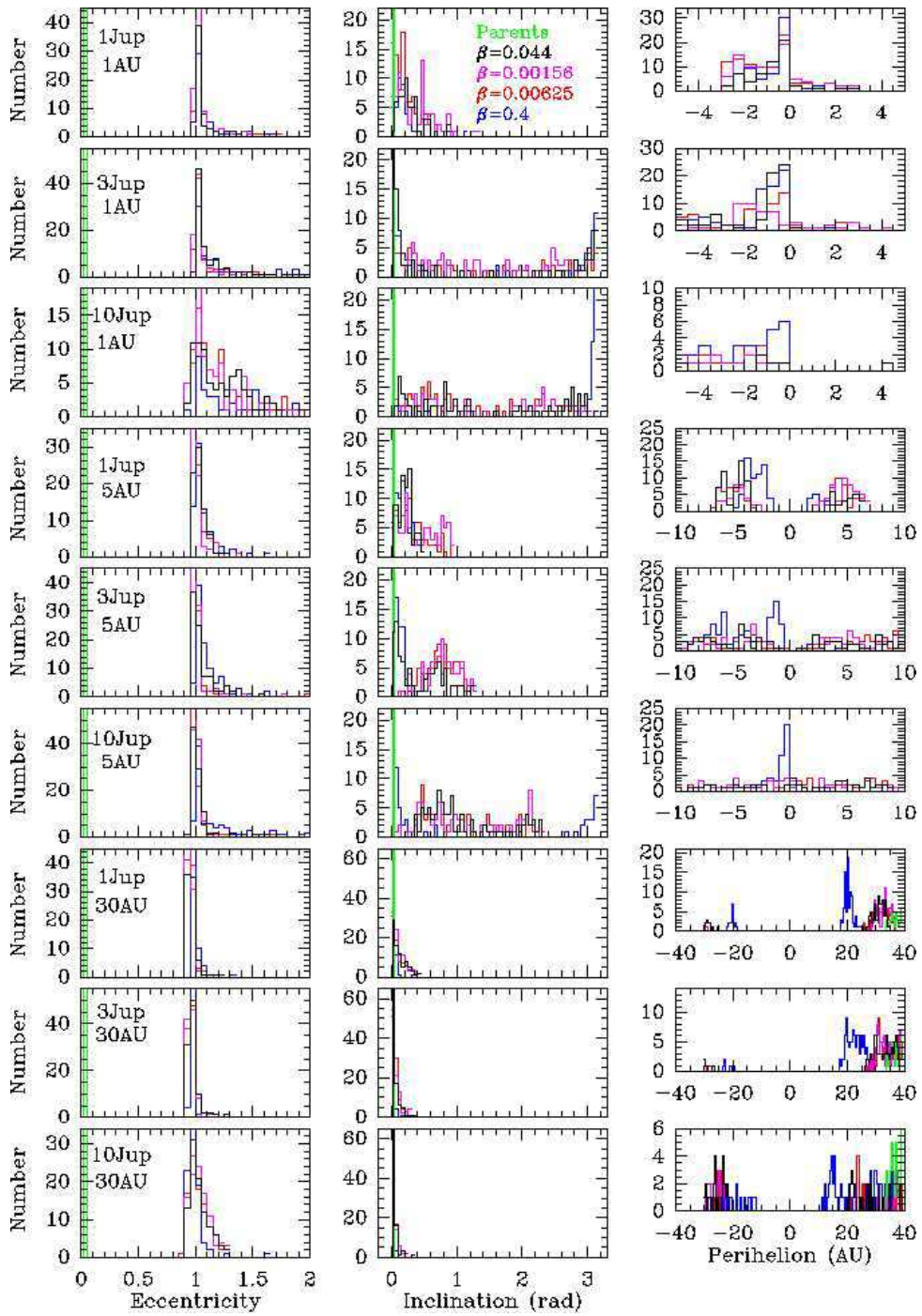


Fig. 7.— Distribution of eccentricity (left), inclination (center) and perihelion (right) of the ejected particles that reach 1000 AU, for three different particles sizes, corresponding to β -values of 0.044 (black), 0.00156 (magenta), 0.00625 (red) and 0.4 (blue). The green lines show the distributions for the parent bodies with $a=35\text{--}50$ AU, $e=0\text{--}0.05$ and $i=0\text{--}0.05$ radians.

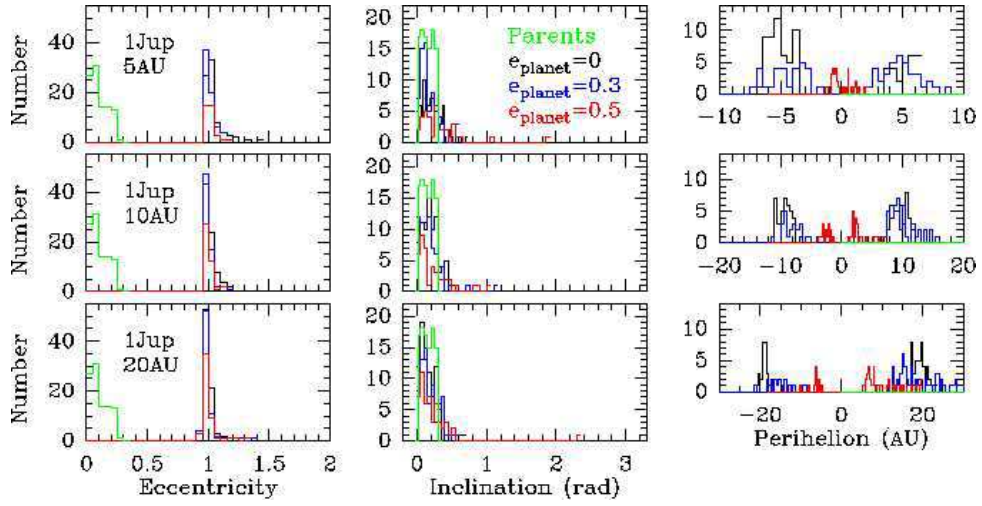


Fig. 8.— Distribution of eccentricity (left), inclination (center) and perihelion (right) of the ejected particles that reach 1000 AU (with $\beta=0.044$), for a system with a $1M_{Jup}$ planet with eccentricity of 0 (black), 0.3 (blue) and 0.5 (red). The green lines show the distributions for the parent bodies with $a=35\text{--}50$ AU, e such that perihelion= $35\text{--}50$ AU and $i=0\text{--}17^\circ$.

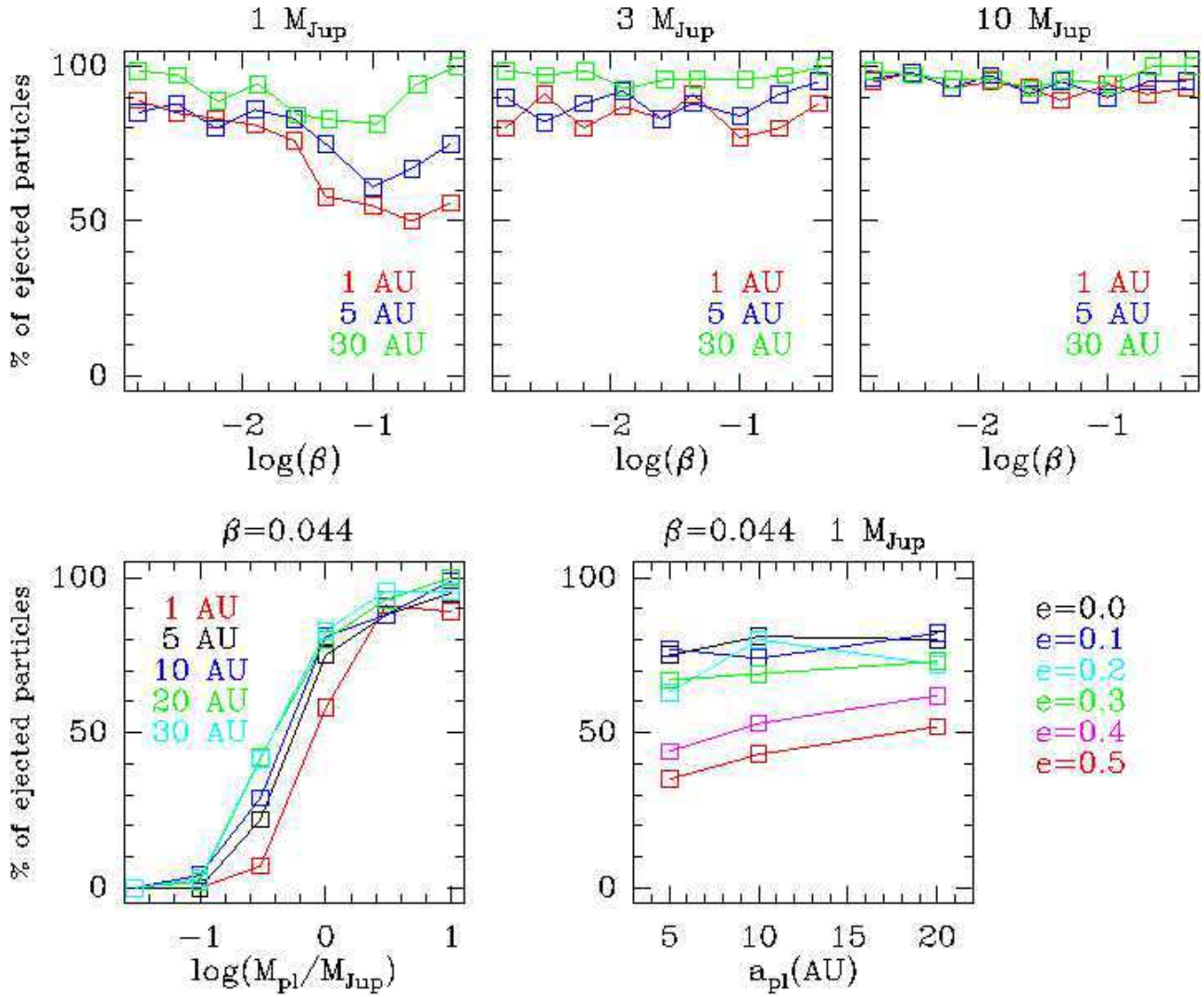


Fig. 9.— Percentage of ejected particles (n_{1000}) as a function of planet’s mass, planet’s semimajor axis and eccentricity and particle size. The models with the planet at 30 AU were based on 70 dust parent bodies between 40 and 50 AU.

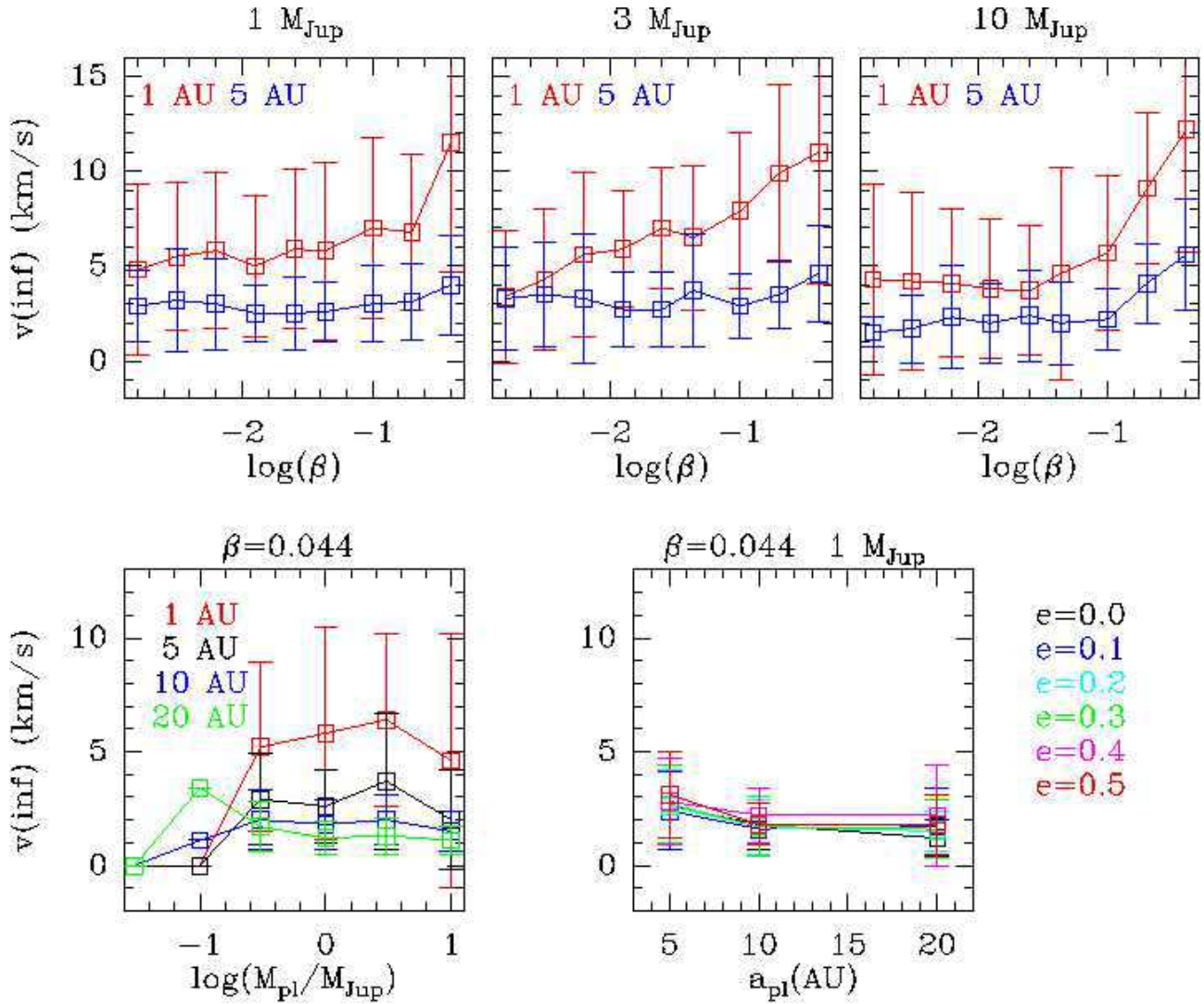


Fig. 10.— Velocity at infinity of particles in hyperbolic orbits as a function of planet’s mass, planet’s semimajor axis and eccentricity and particle size.

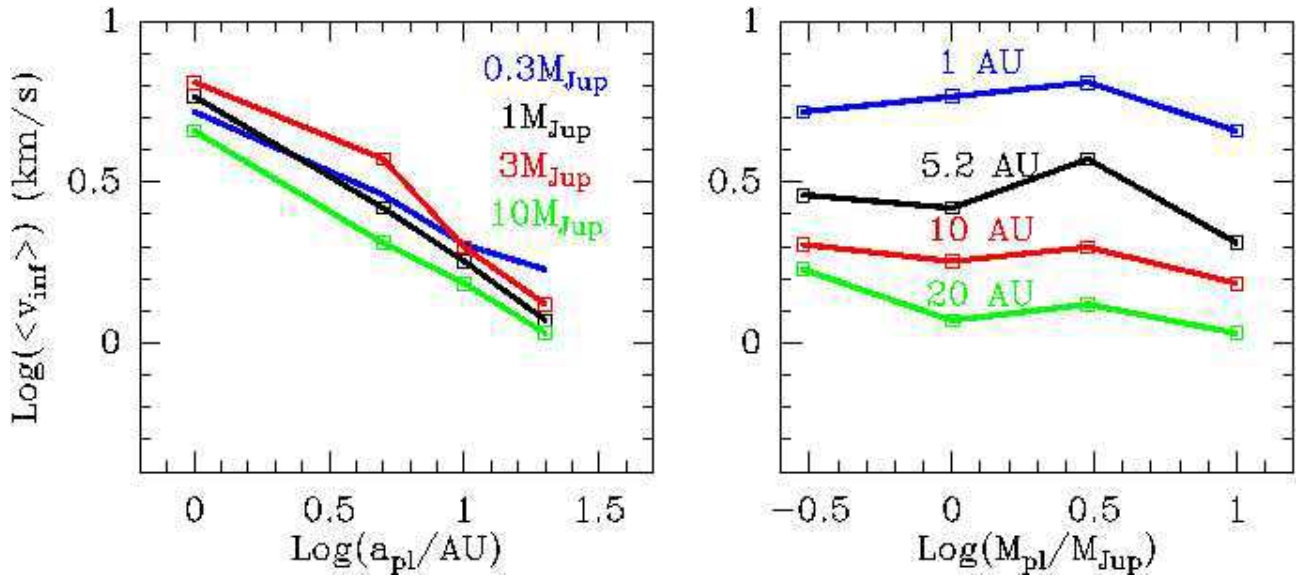


Fig. 11.— Logarithmic plot of the average velocity at infinity of ejected particles of $\beta=0.044$ as a function of planet semimajor axis and planet mass. (left) The blue, black, red and green lines correspond to planet masses of $0.3M_{\text{Jup}}$, $1M_{\text{Jup}}$, $3M_{\text{Jup}}$ and $10M_{\text{Jup}}$, respectively. (right) The blue, black, red, green and light blue lines correspond to models with a planet at 1AU, 5.2 AU, 10 AU and 20 AU, respectively. The parent bodies of the dust particles are distributed like the KBOs, with $a=35\text{--}50$ AU, e such that perihelion= $35\text{--}50$ AU and $i=0\text{--}17^\circ$.

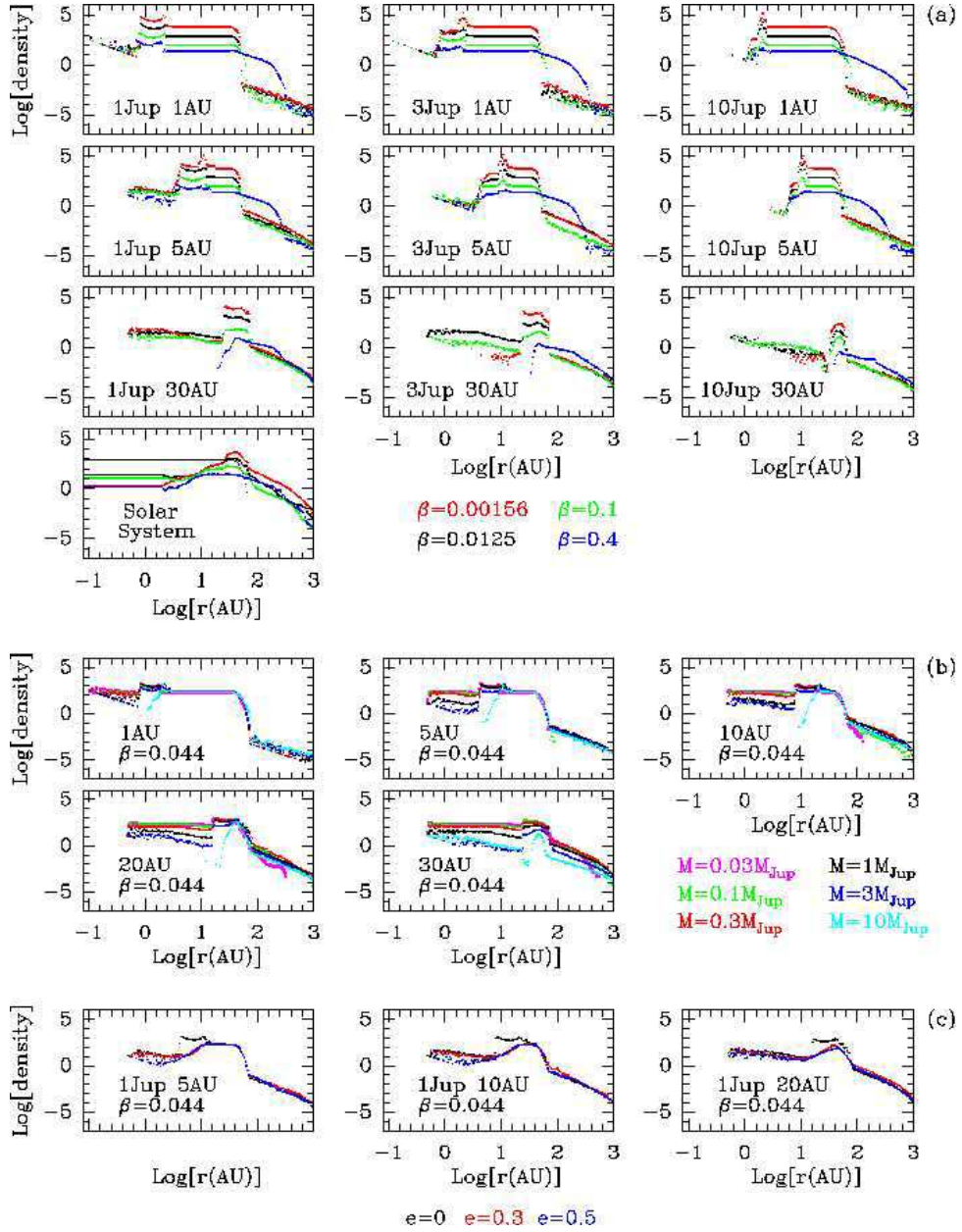


Fig. 12.— (a: top 10 panels) Surface density distributions of dust particles with four different β values (represented by different colors), for different planetary systems (indicated in the individual panels). The units are number of particles per AU² for a dust production rate of 100 particles per 1000 years (to be later scaled to the correct dust production rate or total disk mass). (b: middle 5 panels) Surface density distributions of dust particles with $\beta=0.044$, for different planet masses (represented by different colors), located at five different semimajor axes (indicated in the individual panels). (c: bottom 4 panels) Surface density distributions of dust particles with $\beta=0.044$ and a $1M_{Jup}$ planet, located at four different semimajor axes (indicated in the individual panels), and with three different eccentricities (represented by different colors).